


Article

Textile Wastewater Purification Using an Elaborated Biosorbent Hybrid Material (*Luffa-Cylindrica-Zinc Oxide*) Assisted by Alternating Current

Amina Othmani ^{1,2}, Aida Kesraoui ¹, Roberto Boada ³ , Mongi Seffen ^{1,*}  and Manuel Valiente ^{3,*}

¹ Laboratory of Energy and Materials (LabEM): LR11ES34, Higher School of Science and Technology of Hammam Sousse, University of Sousse, 4011 Hammam Sousse, Tunisia

² Faculty of Sciences of Monastir (Monastir University), 5000 Monastir, Tunisia

³ GTS-UAB Research Group, Department of Chemistry, Faculty of Science, Universitat Autònoma Barcelona, 08193 Bellaterra, Spain

* Correspondence: mongiseffen@yahoo.fr (M.S.); Manuel.Valiente@uab.cat (M.V.); Tel.: +216-26554812 (M.S.)

Received: 31 May 2019; Accepted: 22 June 2019; Published: 27 June 2019



Abstract: This paper aims to synthesize hybrid materials with high pollutant-uptake capacity and low cost based on *Luffa cylindrica* (*L.C*) and different percentage of Zn^{2+} in the presence and absence of alternating current (AC). Physico-chemical, morphological and structural characterizations of the hybrid materials were performed by Boehm method, point zero charge (pH_{pzc}), infrared characterizations (IR), scanning electron microscopy (SEM), energy-dispersive spectroscopy and X-ray photoelectron spectroscopy. The efficiency of the designed hybrid materials was optimized based on their performance in water depollution. Methylene blue (MB) and industrial textile wastewater were the investigated pollutants models. IR characterizations confirmed the fixation of Zn^{2+} onto the *L.C* by the creation of Zn-OH, Zn-O and Zn-O-C bonds. Boehm titration showed that the fixation of Zn^{2+} onto *L.C* is accompanied by an increase of the basic functions of its surface and subsequently an increase in the pH_{pzc} . SEM results confirmed the fixation of Zn^{2+} onto the *L.C* coupling AC with biosorption showed an increase in the adsorbed amount of MB and speed when adding the 4% of Zn^{2+} compared to the pure *L.C* the Q_m shifted from 3.22 to 9.84 and 8.81 mg/g, respectively, for hybrid materials synthesized under AC, in absence of AC and pure *L.C*.

Keywords: alternating current; coupling; hybrid material; biosorption; wastewater reuse

1. Introduction

Textile dyeing wastewaters are classified among the most highly toxic effluents [1,2]. Numerous processes have been suggested for treatment and purification such as biological treatment [3], coagulation-flocculation [4], adsorption [5], ultrafiltration [6], electrocoagulation [7], reverse osmosis [8] and anodic oxidation [9]. The current research was devoted to water remediation through the valorization of the abundant renewable resource of cellulosic fibers [10]. Brown algae [11], *Bacillus macerans* [12], *Posidonia oceanica* [13], corn stigmas [14], *Agave Americana* [15], *Luffa cylindrica* [16], fly ash and red mud [17], raw date pits [18] and *Phragmites australis* [19] are widely used as a natural and cheap biosorbent for a pollutant removal. However, achieving a quick adsorption kinetic with a high possibility of water reuse after filtration absolutely depends on the biosorbent efficiency.

Hybrid materials are praised for not only intermediate properties between mineral and organic matter but also for new interesting behaviors that allow them to be used in several fields of applications. Such domains include catalytic applications, medical and pharmaceutical applications, optoelectronics, the environment, and biomaterials [20,21]. Hybrid materials can be prepared by several methods such

as chemical vapor deposition (CVD) [22], physical vapor deposition (PVD) [23], laser ablation and sputtering [24]. The synthesis of hybrid materials based on cellulose and zinc oxide is the objective of recent studies. Perelshstein et al. (2009) developed a composite based on cotton fibers and zinc oxide. They synthesized the ZnO particles and then deposited them on the cotton surface by ultrasonic irradiation (sonochemical method) [25]. Weili et al. (2010) have succeeded in synthesizing a hybrid matrix based on wurtzite-cellulose ZnO bacteria by the thermal decomposition method. This new hybrid material obtained plays a very important role in improving the photo catalytic activity of anionic dyes such as, orange methyl [26].

However, the techniques used for the synthesis of hybrid materials are expensive. Other researchers have developed less expensive techniques such as the electrochemical method [27], spray pyrolysis [28] and sol-gel process [29]. Recently, Kesraoui et al. (2018) reported that the precipitation method can be a simple and cheap method used for the synthesis of hybrid materials. They have successfully synthesized hybrid material base on *L.C* and metal oxides (ZnO, Al₂O₃). These last showed a good ability for dyes removals compared to the pure *Luffa cylindrica* (*L.C*) [30]. According to literature, the synthesis of hybrid materials based on compounds containing cellulose and ZnO can present interesting properties allows it to be used in several applications.

However, the removal process often requires a lot of time to reach the balance. Therefore, coupling environmental security (there is no transformation of the initial molecule to toxic compounds as for the oxidation process), low cost, final efficiency, and quick process remains a very important stake.

Taking into account these considerations, a set of aims are proposed in this paper, the synthesis of a high performing hybrid material based on *Luffa cylindrica* (*L.C*) and metal oxide with high pollutant-uptake capacity and low cost by an easy precipitation method in absence and presence of alternating current (AC). Since their good affinity for the removal of several pollutants and their interesting physical and chemical properties, *L.C* and ZnO were considered for the synthesis of the hybrid materials [31,32]. Two main pollutants were taken as models in this study; a cationic dye the methylene blue (MB) taken as a model of dye and an industrial textile wastewater. A detailed investigation of the physicochemical, morphological and structural characterizations was carried out using Boehm titration. Also, Drift method, scanning electron microscopy (SEM), Energy-dispersive spectroscopy (EDS), infrared spectroscopy (IR) and X-ray photoelectron spectroscopy (XPS) analysis were performed. The possible pathway of the Zn²⁺ fixation into the *L.C* fibers and the mechanism of possible interaction of MB onto the lignocellulosic surface are suggested. The mathematic modeling was also supplied using the stochastic model of Brouers-Sotolongo.

2. Material and Methods

2.1. Materials

Methylene blue (MB) (purity: 95%) from Fluka™ (manufacturer, Streinheim, Germany), with chemical formula C₁₆H₁₈N₃SCl and molar mass 319.85 g/mol, was chosen as commercial dye model for this study.

Zinc nitrate (Zn(NO₃)₂·6H₂O; Hexahydrate Purified), sodium chloride (NaCl), sodium bicarbonate (NaHCO₃), sodium carbonate (Na₂CO₃) and sodium hydroxide (NaOH) (purity 99%) were obtained from LOBA CHEMIE (Wodehouse road, Mumbai, India).

The biosorbent used for the synthesis of the hybrid material was fruits of Tunisian *Luffa cylindrica* fibers. This biosorbent was purchased at the local market Sousse. The chemical composition of these fibers was determined by Kesraoui et al. (2016). These fibers are composed of 54% of cellulose, 11% of lignin, 5% of pectin, 7% of fats and waxes and 23% hemicelluloses [33].

2.2. Methods

2.2.1. Biosorbent and Adsorbate Preparation

Tunisian *Luffa cylindrica* (*L.C*) was chosen as a natural biosorbent in this paper. The preparation of this biosorbent consisted of cutting the fibers finely, washing them several times to remove all impurities and drying them at 70 °C until the material was completely dried. As for the adsorbate preparation, it consisted of dissolving 10 mg of MB in 1 L of distilled water to obtain the desired concentration (10 mg/L).

2.2.2. Preparation of Hybrid Materials *L.C*+ (1%, 2%, and 4% Zn²⁺) in Presence and Absence of AC

The Zn²⁺ precursors of solution were obtained from (Zn(NO₃)₂·6H₂O (Hexahydrate Purified) Sigma-Aldrich (99%) (Wodehouse road, Mumbai, India).

The preparation of the hybrid material with different percentages of Zn²⁺ (1%, 2%, and 4%) consists in mixing 5 g of *L.C* (size 250 μm) with 0.05, 0.1 and 0.2 g of Zn(NO₃)₂·6H₂O respectively. Each composite was dissolved with the biomass in 100 mL of distilled water at 298 K at pH = 10, under stirring for two hours. The size of the fibers used was chosen after sieving using an electric sifter and after studying the effect of fiber grain size (40, 80, 125 and 250 μm on the biosorption efficiency). Then, the product was washed several times using distilled water to remove the excess of Zn(NO₃)₂·6H₂O which has not been fixed onto the surface of *L.C*. Thereafter, the product obtained was transferred to a sand bath to dry it at 393 K for two hours. A similar experiment was done for the synthesis of the hybrid material under AC using two zinc electrodes (1.3 × 2.5 cm²; purity 99%) immersed into the solution while stirring. The electrical mounting comprising an AC source, a voltmeter to fix the current density at 0.5 A/m² and the voltage at 15 volts.

2.3. Morphological and Crystallographic Characterizations of Hybrid Materials

Morphological and structural characterizations were done in order to characterize the hybrid material synthesized in the presence and absence of AC.

Infrared characterizations (IR) were performed using a Perkin Elmer Spectrum using KBr pellet technique in the frequency range of 4000 to 500 cm⁻¹. Scanning electron microscopy (SEM) was performed using a JEOL JSM 5400 scanning microscope (USA) after coating them with gold using a JEOL JFC-1199E ion sputtering device (USA). Energy dispersive spectroscopy (EDS) was planned to assess the surface elemental compositions of raw and the hybrid materials *L.C* +4% Zn²⁺ using a JEOL JSM 5400 scanning microscope. EDS was performed after coating them with gold using a JEOL JFC-1199E ion sputtering device. X-photoelectron spectroscopy (XPS) measurements were performed at room temperature with a SPECS PHOIBOS 150 hemispherical analyzer (SPECS GmbH, Berlin, Germany) in a base pressure of 5 × 10⁻¹⁰ mbar using monochromatic Al K α radiation (1486.74 eV) as an excitation source.

2.4. Quantitative and Qualitative Characterization of the Pure *L.C* and the Hybrid Material *L.C*-Zn²⁺

The physicochemical characterization of the pure *L.C* and the synthesized hybrid materials was determined by the Drift method and the Boehm titration. The determination of the zero charge point pH (pH_{pzc}) consisted of placing 0.1 g of *L.C* in 30 mL of NaCl solution (0.01 M) at different pH ranging from 2 to 12. The initial pH is obtained by adding a certain amount of NaOH or HCl (1 M). For the first 24 h, the pH must be measured and then this operation must be repeated during the second 24 h in order to register the difference in pH. By plotting the pH_f = f (pH_i) curve, the pH_{pzc} corresponds to the intersection of this curve with the straight line pH_f = pH_i [34].

The determination of acid-basic properties by Boehm method consisted in bringing into contact 0.5 g of each lignocellulosic material with 25 mL of one of these bases: NaHCO₃, Na₂CO₃ and NaOH

(0.1 M) for 48 h with stirring. 10 mL of each solution was back-dosed with NaOH solution (0.1 M) after acidification with an excess of 0.1 M of hydrochloric acid [35].

2.5. Biosorption of MB onto the Synthesized Hybrid Material

The experiments used for the MB removal by biosorption have been performed in batch reactor by adding 0.1 g of adsorbent (Pure L.C, hybrid material elaborated by precipitation) in 100 mL of MB solution (pH = 10, $C_i = 10$ mg/L, $J = 0.5$ A/m², voltage = 15 volts, T = 298K). The electrical mounting comprising an AC source and a voltmeter. All the analyses were carried out in triplicate.

After biosorption, residual concentrations were determined by UV visible spectrophotometer biochrome Libra S.22 at $\lambda = 663$ nm based on the following equation [36]. Plastic and quartz cuvettes were used for absorbance tests.

$$\text{Dye removal (\%)} = \frac{(C_i - C_t)}{C_i} \times 100 \quad (1)$$

where C_i is the initial dye concentration (mg/L) and C_t is the dye concentration at any time (mg/L).

2.6. Kinetics Studies

The evaluation of the MB biosorption in terms of adsorbed quantity was done following the Equation (2) [37].

$$Q_t = \frac{C_i - C_e}{m} \times V \text{ (mg/g)} \quad (2)$$

where Q_t is the adsorbed quantity at equilibrium time, C_i is the initial MB concentration (mg/L), C_e is the residual MB concentration at any time (mg/L), V is the volume of solution (L) and m is the mass of the adsorbent (g). At equilibrium, C_i is equal to C_e and Q is equal to Q_e [38].

Brouers-Sotolongo (B.S) model was used to fit the experimental data of MB biosorption. The generalized kinetic equation of the Brouers-Sotolongo model has been developed to provide a universal function for the kinetics of complex systems characterized by exponential law and/or power exponent behaviors. This kinetic model unifies and generalizes previous theoretical attempts to describe what is called "fractal kinetics". The mathematical development of this model and its application are presented in Brouers and Sotolongo [39–41].

The pseudo BSf (n, α) sorption kinetics is given by Equation (3):

$$Q_t = Q_e \left[1 - \left(1 + (n-1) \left(\frac{t}{\tau_c} \right)^\alpha \right)^{\frac{-1}{n-1}} \right] \quad (3)$$

where, n is order of the fractional reaction, α is "fractal time" exponent.

τ_c : characteristic time, Q_e : the adsorbed quantity at saturation, Q_t : the adsorbed quantity at any time.

2.7. Evaluation of the Treated Water Qualities

2.7.1. Determination of Chemical Oxygen Demand (COD) and Total Organic Carbon (TOC)

The global mineralization was determined by measuring the chemical oxygen demand (COD) by a photometric method. The % COD removal can be estimated by (Equation (4)) [37].

$$\text{COD removal (\%)} = \frac{\text{COD}_i - \text{COD}_t}{\text{COD}_i} \times 100 \quad (4)$$

where COD_i is the initial COD (g/L O₂) and COD_t is the residual COD at any time (g/L O₂).

The total organic carbon (TOC) in the solutions of MB and industrial wastewater was measured by a TOC analyzer (HACHIL, 550-TOC-TN model, Schwerte, Germany) and the TOC removal can be estimated as follows:

$$\text{TOC removal (\%)} = \frac{\text{TOC}_i - \text{TOC}_t}{\text{TOC}_i} \times 100 \quad (5)$$

where, TOC_i and TOC_t are respectively the initial total organic carbon and the total organic carbon obtained after fixed time t of electrolysis treatment (ppm C.O).

2.7.2. Germination Tests

The phytotoxicity test consists in the determination of the inhibitory effect of the treated water on the germination and growth potential of lettuce based on the GI. All sample experiments, including reference (pure water), were tripled. The results obtained are finally expressed according to the following relation [42]:

$$\text{GI(\%)} = \frac{\text{number of seeds sprouted in the sample}}{\text{number of seeds sprouted in the reference}} \times \frac{\text{average length of root in the sample}}{\text{average root length in the reference}} \times 100 \quad (6)$$

3. Results and Discussion

3.1. Surface Characterizations

3.1.1. Energy-Dispersive Spectroscopy (EDS) Analysis

The zinc deposit was analyzed with EDS (Table 1). Carbon and oxygen were the major compounds of *L.C* and hybrid materials due to their chemical composition (cellulose, hemicellulose, and lignin). In addition, the appearance of the Zn atom confirmed its fixation onto the surface of *L.C*. The AC enhanced the distribution of Zn^{2+} into the *L.C* fibers where the rates according to the mass of Zn reached about 1.19% and 0.95% respectively for the hybrid material synthesized in presence and absence of AC.

Table 1. Percentages by mass of the chemical elements present on the fiber surface of the raw *Luffa cylindrica* (*L.C*) and the hybrid materials *L.C* + 4% Zn^{2+} and *L.C* + 4% Zn^{2+} + AC.

	C	O	Na	Mg	Al	Si	P	S	Cl	Ca	Mo	Zn
<i>L.C</i>	54.46	40.60	0.45	0.38	0.80	1.10	0.29	0.00	0.35	1.40	0.17	0.00
<i>L.C</i> + 4% Zn^{2+} + AC	57.01	35.64	0.00	0.38	4.78	0.00	0.00	0.00	1.00	0.00	0.00	1.19
<i>L.C</i> + 4% Zn^{2+}	50.43	40.18	0.00	0.79	4.58	2.40	0.00	0.08	0.59	0.00	0.00	0.95

3.1.2. Infrared Spectroscopy (IR)

Figure 1 shows that the spectrum of pure *L.C* has a vibration band at 3438 cm^{-1} which corresponds to the O-H bond present in cellulose, hemicellulose, and lignin. In the presence of different percentages of Zn^{2+} (1%, 2%, and 4%), obtained by precipitation (Figure 1a), the band of hydroxyl groups is observed at 3435, 3430 and 3414 cm^{-1} . The decrease in the position of these bands can be attributed to the presence of elongation vibration of the Zn-OH bond, between Zn^{2+} and cellulose [43]. These results indicate that the hydroxyl groups have a strong interaction with Zn^{2+} .

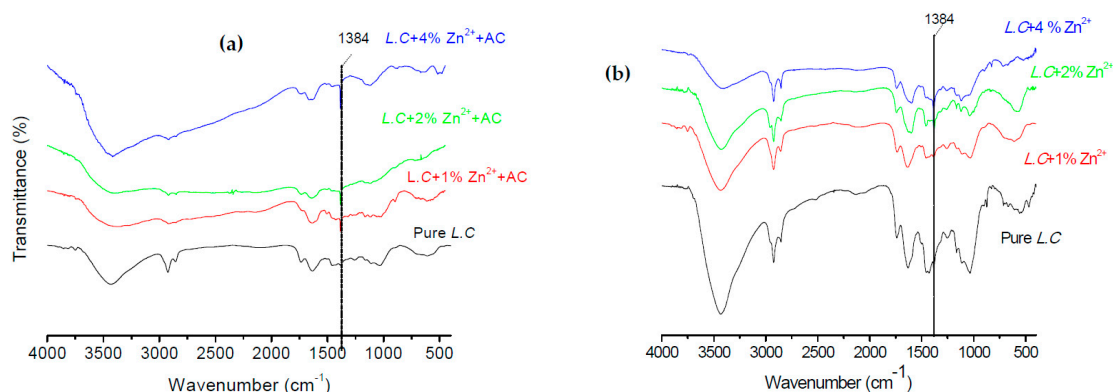


Figure 1. Spectrum of pure *L.C* and *L.C* + (1%, 2% and 4% Zn^{2+}) synthesized (a) in presence of alternating current (AC) and (b) in the absence of AC.

The appearance of 1383 peaks at 4% *L.C*- Zn^{2+} is probably due to symmetric Zn-O-C vibration [44]. The bands at 1032.56, 1016.77 and 1016 cm^{-1} , which correspond to the vibration of the C-O bond, increase in intensity, which can be attributed to the appearance of the Zn-O-C bond.

Based on Figure 1b, the rising of the percentages of Zn^{2+} added during the synthesis of hybrid materials by precipitation under AC caused the decrease of the position of the band of hydroxyl groups. This last passed from 3438 cm^{-1} to 3430, 3427 and 3420 cm^{-1} . This decrease in position can be attributed to the formation of Zn-OH stretching vibration [45].

Furthermore, we note the appearance of the Zn-O bond is proven by the appearance of peaks at 1383, 517 and 485 cm^{-1} [46].

The bonds located at 1032.56, 1016.77 and 1016 cm^{-1} correspond to the vibration of the C-O bond. An increase in the intensity of these bonds was shown when adding the Zn^{2+} . This increase can be explained by the appearance of the Zn-O-C bond.

The band located at 1383 cm^{-1} presents the main difference between the IR spectrum obtained the hybrid materials synthesized in the presence and absence of AC. For the hybrid material synthesized under AC, the band at 1383 cm^{-1} appears from 1% of Zn^{2+} . While the hybrid material synthesized by precipitation this band appears only for 4% of Zn^{2+} . This behavior is probably due to the effect of AC on the fixation of Zn^{2+} ions into the *L.C* fibers by the creation of Zn-O-C bonds.

3.1.3. X-ray Photoelectron Spectroscopy (XPS) Analysis

XPS measurements were performed in order to clarify the main difference between the syntheses of the hybrid material with and without AC. Based on IR characterizations; Zn is strongly bound to the lignocellulosic surface by OH hydroxyl ions which are confirmed by the presence of O-Zn-O and O-Zn bonds. Figure 2 displays the main XPS results for the hybrid material *L.C* + 4% Zn^{2+} synthesized in the presence and absence of AC. The high-resolution XPS spectra of C(1s), O(1s), Zn(2p), Zn LMM⁺ show noticeable differences between the material synthesis by the two methods. However, neither of them showed any impurities. The C(1s) peak, depicts a chemical shift by ± 0.5 eV in comparison with the C(1s) spectra observed for the hybrid material synthesized in absence of AC (not AC) (282.5 eV) towards a relatively high binding energy positioned at 283 eV specific to C=O and O-C-O [47]. Similar behavior was observed for the O(1s) peak which is positioned at the binding energies of 529.9 and 531.2 eV for the hybrid material *L.C* + 4% Zn synthesized in absence and presence of AC, respectively. These contributions can be assigned to O^{2-} ions in the Zn-O bonding and to O-H groups of adsorbed water molecules [48]. The four peaks observed at the binding energies of 1017.5, 1020 and 1040 and 1044.5 eV, correspond respectively to the zinc oxide (ZnO) and the spin orbit of Zn ($2p_{3/2}$) and Zn ($2p_{1/2}$) for the material synthesized in absence of AC [48]. In presence of AC, two main peaks located at 1021 and 1043.5 eV are assigned to the Zn($2p_{3/2}$) and Zn($2p_{1/2}$) energy levels.

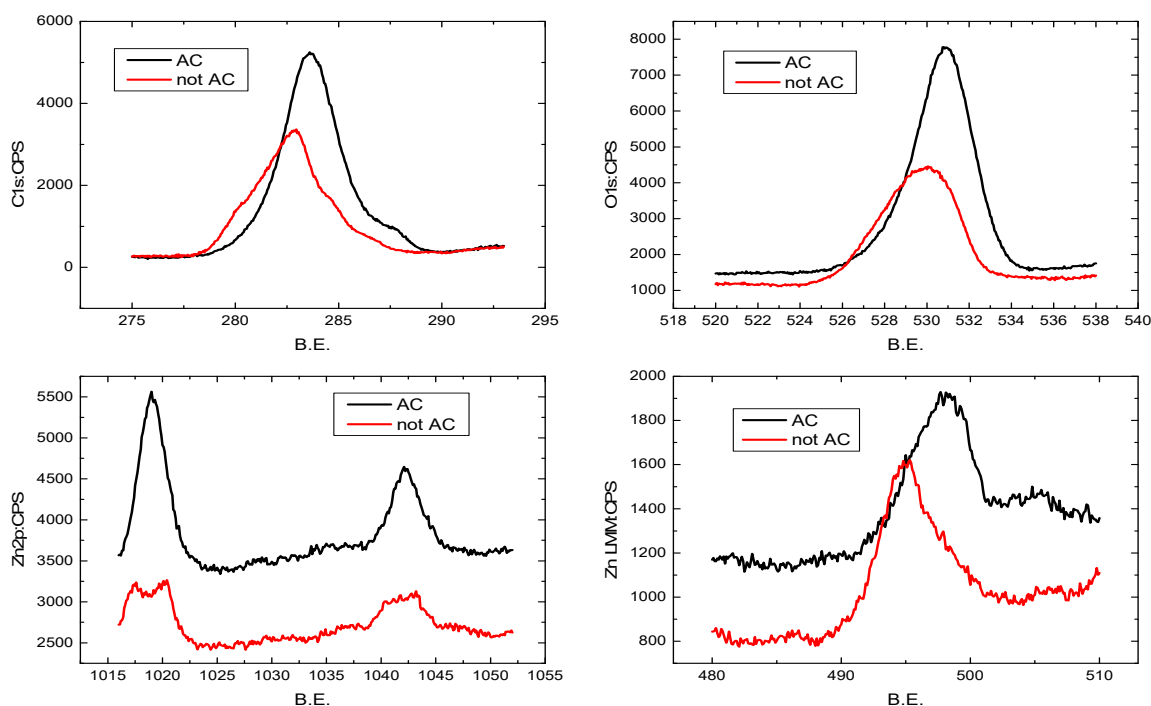


Figure 2. Spectra of C1s, O 1s, Zn 2p and Zn LMM of various morphologies of *L.C* + 4% Zn^{2+} synthesized in presence of AC (-) and absence of AC (not AC -).

Both of these were symmetrical and narrow, indicating the absence of the zinc oxide. Despite this difference, these peaks of the Zn(2p) detected in both hybrid materials are related to Zn-O bonding as confirmed by previous studies [49]. Furthermore, we determined a small offset followed by a big discrepancy in terms of the intensities of peaks which were higher in case of the use of AC. These findings indicated that the obtained Zn does not occur in the same oxidation state and even if they are similar in number. It can also be attributed to the depth distribution of the atoms. This increase in intensity is explained by the diffusion of atoms towards the surface which was more pronounced compared to the hybrid material synthesized without AC. This behavior might stem from the difference in the local chemical environment. It can also be directly related to the number of atoms in the corresponding chemical state, which is confirmed by the signal Zn LMM Auger region. Another possibility is the sharing of the element with its neighbor atoms which applied a crystal field on it. This can also be interpreted in terms of the asymmetry in the bond arrangement which can create extra pressure on the element—so, the binding energy required for the ejection of the electron is slightly higher than its previous case. In the light of these results, we confirm the fixation of Zn^{2+} onto the *L.C* by the creation of Zn-O bond as proven by IR characterizations for both methods used for the synthesis of the hybrid material. However, the environment of Zn bonding is slightly different.

3.1.4. Scanning Electron Microscopy (SEM) Analysis

SEM characterizations were performed to gain further insight into the distribution of Zn^{2+} obtained from $(Zn(NO_3)_2 \cdot 6H_2O)$ on the *L.C* surface by precipitation in presence and absence of AC. Figure 3 shows the obtained micrograph of the pure *L.C* (Figure 3a), hybrid material (*L.C* + 4% Zn^{2+}) synthesized by precipitation (Figure 3b), and hybrid material (*L.C* + 4% Zn^{2+}) synthesized under AC (Figure 3c). *L.C* presents a rough structure and a homogeneous appearance which is formed by bonded multicellular fibers (Figure 3a). This indicates that the existence of a large number of hydroxyl groups could provide effective interaction between *L.C* and Zn^{2+} [26,50]. Figure 3b,c refer to the hybrid material (*L.C* + 4% Zn^{2+}) synthesized in the absence and presence of AC. Here the Zn^{2+} deposit is well visible and well-fixed onto the *L.C* and exhibits good dispersion without significant aggregation. The use of AC has enhanced the distribution of Zn^{2+} into the *L.C* fibers.

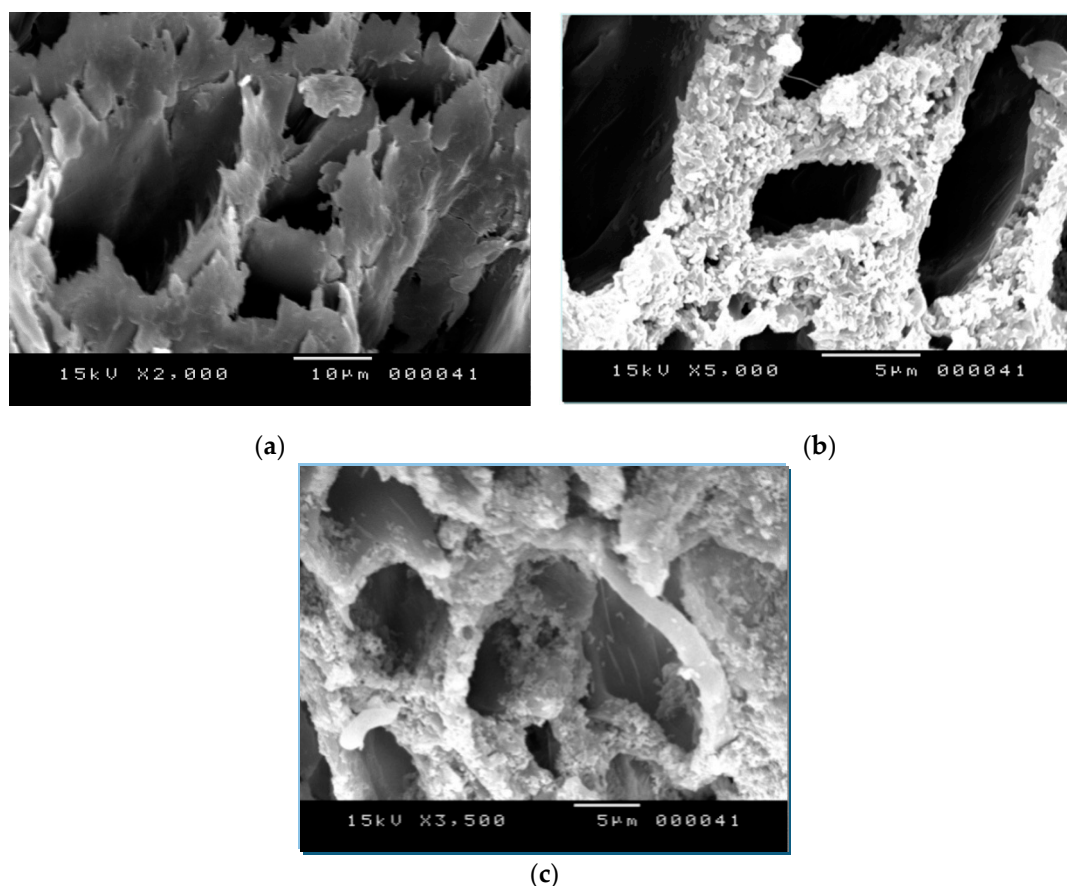


Figure 3. Images of (a) pure *L.C*, (b) *L.C* + 4% Zn^{2+} synthesized in absence of AC, (c) *L.C* + 4% Zn^{2+} synthesized in presence of AC.

3.1.5. Surface Chemical Analysis of Pure *L.C* and Hybrid Materials

Table 2 shows the main pH_{pzc} values obtained for the pure *L.C* and the synthesized hybrid materials. The presence of zinc increased the pH_{pzc} which made the fibers slightly basic. In addition, pH_{pzc} increases with increasing the percentage of zinc added.

Table 2. pH_{pzc} of hybrid material synthesized in absence and presence of AC.

Samples	pH_{pzc} under AC	pH_{pzc} without AC
Pure <i>L.C</i>	7.38 ± 0.021	7.38 ± 0.021
<i>L.C</i> + 1% Zn^{2+}	7.57 ± 0.008	7.41 ± 0.016
<i>L.C</i> + 2% Zn^{2+}	7.77 ± 0.005	7.69 ± 0.012
<i>L.C</i> + 4% Zn^{2+}	7.96 ± 0.005	7.86 ± 0.012

The pH_{pzc} of *L.C* is equal to 7.38. This result shows that the surface of *L.C* has a positive charge at pH values below pH_{pzc} and should, therefore, be able to adsorb anions and a negative charge at pH values above pH_{pzc} and should, therefore, be able to adsorb cations [51].

On the other hand, according to Table 3, for the pure *L.C*, the amount of base and the total amount of acid groups are approximately equal. These results suggest that *L.C* fibers have an amphoteric character. This amorphous character confirms the result found by the pH_{pzc} (7.38).

Table 3. Different functional groups obtained on the adsorbent surfaces.

Adsorbent	Acidic Function ($\times 10^{-4}$ mmol/g)				Basic Function ($\times 10^{-4}$ mmol/g)
	Carboxylic	Phenolic	Lactonic	Total	
Pure <i>L.C</i>	0.397 ± 0.002	0.935 ± 0.003	0.178 ± 0.008	1.510 ± 0.005	1.560 ± 0.0008
<i>L.C</i> + 1% Zn^{2+}	0.280 ± 0.002	0.790 ± 0.004	0.200 ± 0.001	1.280 ± 0.001	1.610 ± 0.0005
<i>L.C</i> + 2% Zn^{2+}	0.201 ± 0.002	0.544 ± 0.003	0.310 ± 0.002	1.055 ± 0.002	1.700 ± 0.0004
<i>L.C</i> + 4% Zn^{2+}	0.170 ± 0.002	0.400 ± 0.002	0.430 ± 0.002	1.000 ± 0.001	1.810 ± 0.0007
<i>L.C</i> + 1% Zn^{2+} + AC	0.220 ± 0.001	0.503 ± 0.001	0.270 ± 0.002	0.993 ± 0.0009	1.560 ± 0.0006
<i>L.C</i> + 2% Zn^{2+} + AC	0.198 ± 0.0008	0.399 ± 0.002	0.390 ± 0.0008	0.987 ± 0.0006	1.790 ± 0.0003
<i>L.C</i> + 4% Zn^{2+} + AC	0.155 ± 0.001	0.236 ± 0.001	0.511 ± 0.0005	0.902 ± 0.0005	1.920 ± 0.0001

The carboxylic and phenolic functions of hybrid materials synthesized under AC (*L.C* + Zn^{2+} + AC) are lower than those synthesized in absence of AC (*L.C* + Zn^{2+}) (0.155 ± 0.001 and 0.170 ± 0.002 for the carboxylic functions, 0.400 and 0.230 for the phenolic functions, respectively). These findings confirm the increase of pH_{pzc} obtained during the synthesis of the hybrid material in presence of AC (7.96 ± 0.005) which was slightly higher than that obtained during the synthesis in its absence (7.86 ± 0.012). It is apparent that the addition of Zn^{2+} and the use of AC slightly influenced the functional groups of hybrid materials obtained. Such behavior can be explained by the increase in the number of available sites on the surface of the materials, which enhances the uptake capacity of such materials and accelerates the biosorption kinetics.

Furthermore, the basic and lactonic functions of *L.C*- Zn^{2+} + AC are higher than those of *L.C*- Zn^{2+} (1.920 ± 0.0001 and 1.810 ± 0.0007 for basic functions and 0.511 ± 0.0005 and 0.430 ± 0.002 for lactonic functions, respectively). According to Mahdoudi et al. (2015), the increase in basic functions is probably due to partial or total deprotonation of the active sites of the hybrid material. Therefore, the fixation of zinc onto *L.C* is accompanied by an increase of the basic functions of its surface and subsequently an increase in the pH_{pzc} . The dissociation of the surface oxygen groups of the acidic groups (carboxylic, lactone and phenol) confers a negative charge on the surface of *Luffa cylindrica*. Thus, the surface acid sites are of Brönsted type [52]. With regard to the positive charge, this may result from the existence of basic oxygen groups such as pyrones or benzopyran.

3.2. Kinetics of MB Biosorption Assisted by AC

The MB biosorption tests were performed at an initial dye concentration of 10 mg/L, $pH = 10$, a mass of the adsorbent of 0.1 g and a temperature of 298 K, $V = 15$ volts, $J = 0.5$ A/m².

Figure 1 shows that the method of elaboration of the hybrid material has a great influence on the biosorption capacity. Indeed, the adsorbed quantity of the highest MB is obtained by the hybrid material (*L.C* + 4% Zn^{2+} + AC). As a result, the adsorbed amount of MB increased from 3.22 mg/g for pure *L.C* to 8.81 mg/g for *L.C* + 4% Zn^{2+} and 9.84 mg/g for *L.C* + 4% Zn^{2+} + AC. Similarly, the MB removal rates reached about 98.4, 88.1 and 31.4% respectively for the hybrid material *L.C* + 4% Zn^{2+} synthesized in the presence and absence of AC and the pure *L.C* (Figure 4).

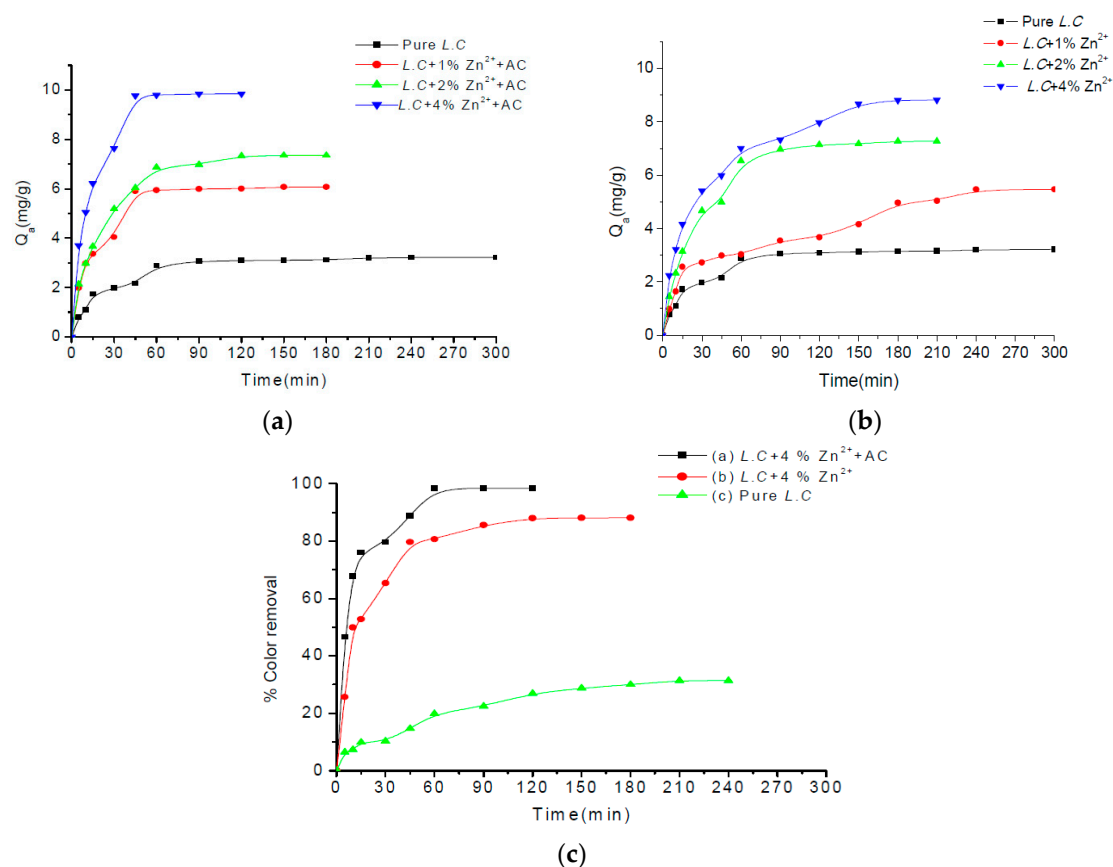


Figure 4. Kinetics of retention of methylene blue (MB) onto different materials used *L.C.*; pH = 10, $C_i = 10$ mg/L, $m = 0.1$ g, $T = 298$ K. (a) hybrid material *L.C.* + 4% Zn²⁺ synthesized in presence of AC, (b) hybrid material *L.C.* + 4% Zn²⁺ synthesized in absence of AC, (c) % color removal using different materials.

The use of AC in the synthesis of the hybrid material for different percentages of Zn²⁺ improved the quantities adsorbed as well as the time required for the process. This behavior can be explained by the facility of the access of pollutants into the biosorbent pores and the availability of more active sites for biosorption offered by the synthesized hybrid materials.

Contrariwise, the best results were obtained for hybrid materials *L.C.* + 4% Zn²⁺ synthesized in the presence and absence of AC as the Q_{max} reached, respectively, 9.83 mg/g and 8.81 mg/g. Interestingly, the high amount of added Zn²⁺ assures the increase of superficial negatively charged groups obtained by lactonic function (as confirmed by Boehm titration). Therefore, this increase of negatively charged groups increased the biosorption capacity.

When comparing biosorption when using hybrid material synthesized in the presence of AC and those synthesized in its absence as well as the pure *L.C.*, definitely, the speed of biosorption and the capacity uptake were greatly enhanced. While the time required for the biosorption of MB is almost lower than that required when using the pure *L.C.* and hybrid materials synthesized in the absence of AC. This is probably due to the existence of the electric field which increased the speed of movement of the molecules of MB and facilitated their access into the active sites.

3.3. UV Characterizations

To forecast the main phenomena that may occur during the MB biosorption, an UV-visible characterization was performed as shown in Figure 5. The characterization was done in order to compare the initially existing bands and the new ones that may appear during the biosorption of MB assisted by AC. The initial MB spectra display three main peaks located at 293,602 and

663 nm corresponding to the chromophore (dimethylamino group) and the aromatic rings in the MB molecule [53]. After MB biosorption, a decrease in the intensity of peaks recorded in the visible range at $\lambda_{\max} = 663$ nm relative to the naphthalene group [54] was observed for all biosorbent used. No new band appeared, thus indicating that no intermediates appeared and confirming that the color removal is probably due to a biosorption and not to an oxidation process which was probably due to the azo groups. It is interesting to note that the biosorption of MB was particularly important by using the hybrid material $L.C + 4\% Zn^{2+}$ synthesized by precipitation under AC (Figure 5a) compared to the pure $L.C$ (Figure 5c) and hybrid material synthesized in absence of AC (Figure 5b). In addition, the biosorption was rapidly obtained and within 120 min and a steady state concentration was achieved indicating a great ability of hybrid material for dye removal. On the contrary, the MB biosorption was tardier and the removal efficiency was lower when using the pure $L.C$ (Figure 5c).

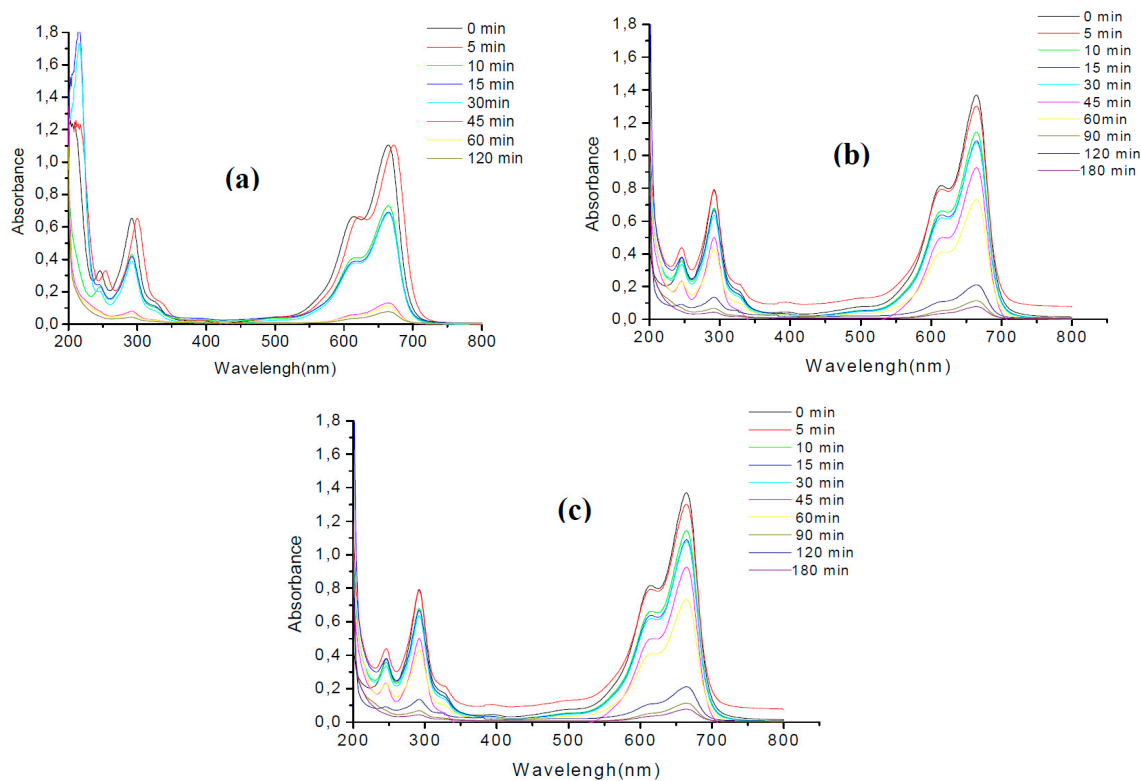


Figure 5. Spectra of MB biosorption assisted by AC using (a) hybrid material $L.C + 4\% Zn^{2+}$ synthesized in presence of AC, (b) hybrid material $L.C + 4\% Zn^{2+}$ synthesized in absence of AC and (c) pure $L.C$, $C_i = 10$ mg/L, pH = 10, $m_{L.C} = 0.1$ g, $V = 0.1$ L, $T = 298$ K.

3.4. Modeling of the Biosorption of MB Assisted by AC Using Brouers Sotolongo (B.S) Model

The biosorption mechanism of MB onto pure $L.C$ and hybrid materials elaborated by precipitation in the presence and absence of AC was studied by B.S model. The surface of the biosorbent is heterogeneous. The functions are distributed randomly hence the need to use a stochastic model (B.S). This model was chosen based on the coefficient of determination (R^2), the non-linear chi-square test (χ^2) and the calculated Q_e (Table 4 and Table S1 in the complementary information).

Table 4. Comparative results for the B.S model.

Biosorbent Used	Q_{exp} (mg/g)	Q_{the} (mg/g)	R^2	χ^2	α	τ_c
Brouers Sotolongo n = 1						
Pure <i>L.C</i>	3.22	4.33	0.9999	0.0001	0.99	91.52
<i>L.C</i> + 1% Zn^{2+} + AC	6.06	5.97	0.9995	0.0005	1.11	56.14
<i>L.C</i> + 2% Zn^{2+} + AC	7.33	7.41	0.9999	0.0005	1.27	47.98
<i>L.C</i> + 4% Zn^{2+} + AC	9.84	9.31	0.9999	0.0001	5.41	36.83
<i>L.C</i> + 1% Zn^{2+}	5.47	5.40	0.9999	0.0001	0.99	59.01
<i>L.C</i> + 2% Zn^{2+}	7.27	7.22	0.9999	0.0004	1.06	49.13
<i>L.C</i> + 4% Zn^{2+}	8.81	8.64	0.9999	0.0001	3.64	39.55

Table 4 shows that B.S model BSf (1, α) presents the best fit to experimental data related to MB biosorption by *L.C* and hybrid materials. Indeed, the B.S model BSf (1, α) has the highest coefficient of determination and the lowest nonlinear chi-square test. In addition, the Q_e calculated by this model gives acceptable values.

The comparison of the values of τ_c calculated from BSf (1, α) shows that *L.C* + 4% Zn^{2+} + AC has the lowest value of τ_c (36.83). These results indicate that the AC synthesized hybrid materials remarkably improve both the adsorption capacity and the reaction rate of pure *L.C*.

On the other hand, the fractal constant α of *L.C* is less than one—which shows that the surface of *L.C* is heterogeneous [55]. Although the fractal constant α of the hybrid materials exceeds one, the kinetic is not clearly fractal [56].

For the hybrid materials, the fractal constant α increases with the increase of the percentage of Zn^{2+} added. The hybrid material elaborated by AC (*L.C* + 4% Zn^{2+}) presents a higher value of α . In fact, Selmi et al. (2018) showed that the fractal constant α increases with the number of functional surface groups [57]. Therefore, the hybrid material elaborated by AC (*L.C* + 4% Zn^{2+}) has the highest number of functional groups.

3.5. Evaluation of the Elaborated Hybrid Material for MB Biosorption: A Comparative Study

To estimate the efficiency of the hybrid material synthesized by the precipitation method in presence and absence of AC and other low-cost material widely used for dye removal, a comparative study in terms of biosorption capacity (Q_m) and efficiency was done as illustrated in Table 5. Results obtained when using the hybrid material *L.C* + (1%, 2%, and 4% Zn^{2+}) synthesized by precipitation under AC are largely higher than those obtained when using the hybrid material synthesized in absence of AC and the other low-cost materials. The Q_m shifted from 3.22 to 8.81 and 9.84 mg/g, respectively, for the hybrid material *L.C* + 4% Zn^{2+} synthesized under AC, the hybrid material *L.C* + 4% Zn^{2+} synthesized in absence of AC and the pure *L.C*. The Q_m increased greatly when adding the 4% of Zn^{2+} compared to the pure *L.C*. These findings can be explained by the high dispersion of active sites due to the availability of a large number of sites. The modification of pure *L.C* by different zinc rates in the presence and absence of AC increased the active sites available for MB retention. Furthermore, the rapid change in current direction has enhanced the access of pollutants into the biosorbent pores—which explained the main difference between rates achieved in both cases.

Table 5. Comparison of biosorption characteristics between hybrid material synthesized and other studied biosorbents used for MB biosorption.

Biosorbents/MB	Q _m (mg/g)	References
<i>Luffa cylindrica</i>	3.9	This study
<i>L.C</i> + 1% Zn ²⁺	5.47	This study
<i>L.C</i> + 2% Zn ²⁺	6.55	This study
<i>L.C</i> + 4% Zn ²⁺	8.77	This study
<i>L.C</i> + 1% Zn ²⁺ + AC	6.06	This study
<i>L.C</i> + 2% Zn ²⁺ + AC	7.33	This study
<i>L.C</i> + 4% Zn ²⁺ + AC	9.01	This study
Algae <i>Caolina</i>	6	[57]
Langsat peel	8	[58]
Agave Americana	6	[59]
Posidonia Oceanica	5.51	[60]
Phragmites Australis	6.31	[61]

3.6. Evaluation of the Synthesized Hybrid Material on the Purification of Industrial Textile Wastewater

Some experiments were performed in order to foresee the variation of pH, COD, turbidity, TOC and processing time during the purification of industrial wastewater (Table 6). In fact, the treated wastewater is composed of sodium carbonate, caustic soda, sodium sulfate, sea salt, wetting agent, reactive dyes, chlorine, and enzymes. *L.C* + 4% Zn²⁺ synthesized in the presence and absence of AC and the pure *L.C* were evaluated for the purification.

Table 6. Comparative results obtained for the purification of industrial textile wastewater.

Parameters	Industrial Textile Wastewater			
	Biosorbent Used	Pure <i>L.C</i>	<i>L.C</i> + 4% Zn ²⁺	<i>L.C</i> + 4% Zn ²⁺ + AC
pH _i		11.22	11.22	11.22
pH _f		8.99	8.08	8
COD _i (mg/L)O ₂		1265	1265	1265
COD _f (mg/L)O ₂		597	297	159
COD removal (%)		52.80	76.5	87.43
Turbidity _i (NTU)		11.70	11.70	11.70
Turbidity _f (NTU)		4.58	2.23	1.99
Turbidity removal (%)		60.85	80.94	82.99
TOC _i (ppm(C.O))		28.9	28.9	28.9
TOC _f (ppm(C.O))		11.9	3.2	2.29
TOC removal (%)		58.82	88.92	92.07
Processing time (min)		300	240	180

Results show that the hybrid material (*L.C* + 4% Zn²⁺) synthesized under AC is more efficient when synthesized in the absence of AC and pure *L.C* for purification of industrial textile wastewater.

The % of TOC, % of COD and the % of turbidity removals obtained for the hybrid material synthesized in presence of AC were higher than those obtained by hybrid material *L.C* + 4% Zn²⁺ synthesized in absence of AC and pure *L.C*.

Both 87.43% of COD and 92.07% of TOC were removed from the industrial textile wastewater when using the hybrid material *L.C* + 4% Zn²⁺ synthesized in presence of AC. 52.80% of COD and 58.82% of TOC were removed from the tested industrial wastewater when using the pure *L.C*. 76.5% of COD and 80.94% of TOC were removed when using the hybrid material *L.C* + 4% Zn²⁺ synthesized in absence of AC, for the purification of the industrial wastewater.

The same behavior was observed for the % of turbidity removal. Values reached about 60.85 for pure *L.C*, 80.94% for the hybrid material (*L.C* + 4% Zn²⁺) synthesized in absence of AC and 82.99%, respectively, for hybrid material (*L.C* + 4% Zn²⁺) synthesized in presence of AC.

While for pH, both *L.C* and hybrid materials (*L.C* + 4% Zn^{2+}) had a significantly poor effect. This considerable fluctuation in the evaluated parameters may be attributed to the increase of the sites available for the color retention offered by the elaborated hybrid material as indicated by the Brouers-Sotolongo modeling. This analysis revealed that almost all of the parameters satisfied the Tunisian standards TN-106-02 indicating that the treated wastewater can be discharged to any receiving water body.

3.7. Phytotoxicity Test

In order to evaluate the suitability of the raw and treated industrial textile wastewater for agricultural use, a phytotoxicity test was done. The evolution of the germination index (GI), the length of root, stem and leaf of lettuce using distilled water, raw and treated industrial textile wastewater was evaluated. The most used model for weeds is lettuce "*Lactuca Sativa*". It has been used extensively thanks to its fast germination and high sensitivity for a large variety of pollutants. Furthermore, it is often used for the examination of plants interaction in an aquatic environment [62,63].

Figure 6 (Figure S1 in the complementary information) presents the main results obtained. The germination index (GI) of the initial concentrations of the tested industrial wastewater was equal to 29.87%. After biosorption assisted by AC, the percentage of the germination index increased indicating a decrease in the toxicity of the wastewater tested. It reached respectively 72.33, 59.79, and 52.14%, respectively, when using the hybrid material (*L.C* + 4% Zn^{2+}) synthesized in presence of AC, the hybrid material *L.C* + 4% Zn^{2+} synthesized in presence of AC and the pure *L.C*. Results showed that all GI were higher than 50%, indicating the purity of the treated wastewater and its suitability to agricultural use.

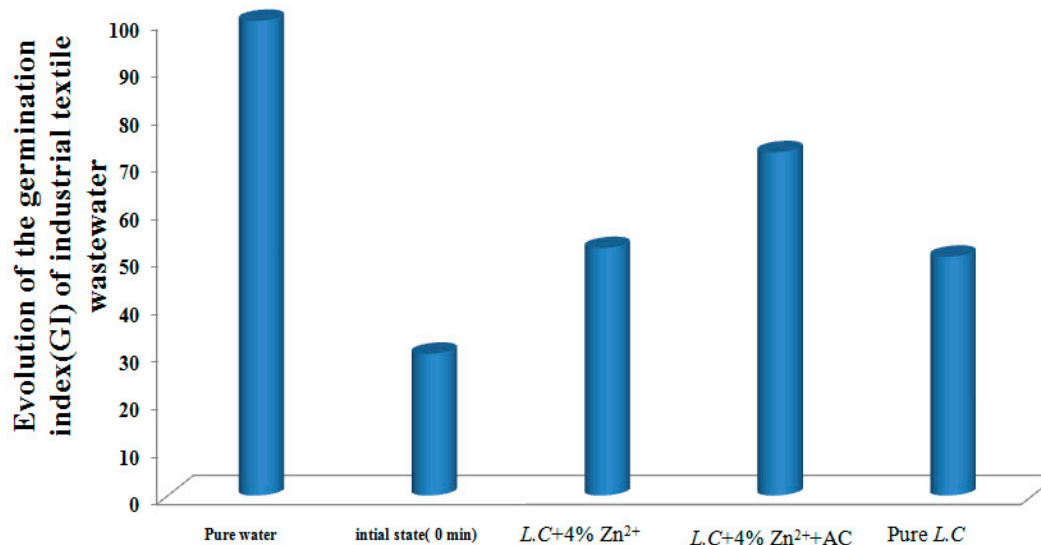


Figure 6. Evolution of the % GI after coupling biosorption with AC using pure *L.C* and hybrid material *L.C* + 4% Zn^{2+} synthesized in presence and absence of AC.

3.8. Mechanism of Biosorption of MB

An assumption of the pathway of the fixation of Zn^{2+} ions onto the *L.C* fibers and the possible interactions between MB and the synthesized hybrid material were predicted as shown in Figures 7 and 8.

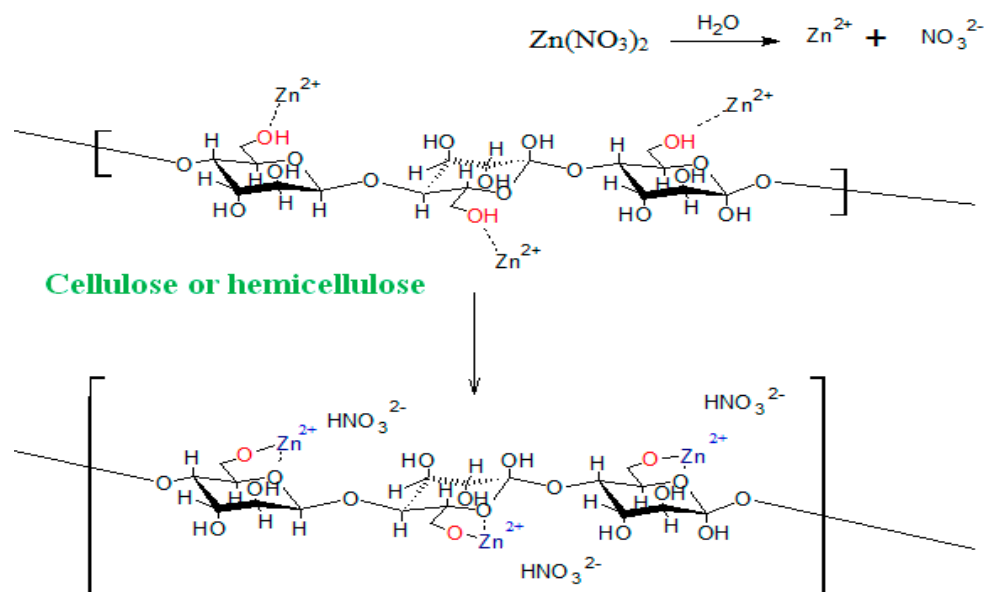


Figure 7. Possible pathway for the fixation of Zn^{2+} onto the *L.C* surface.

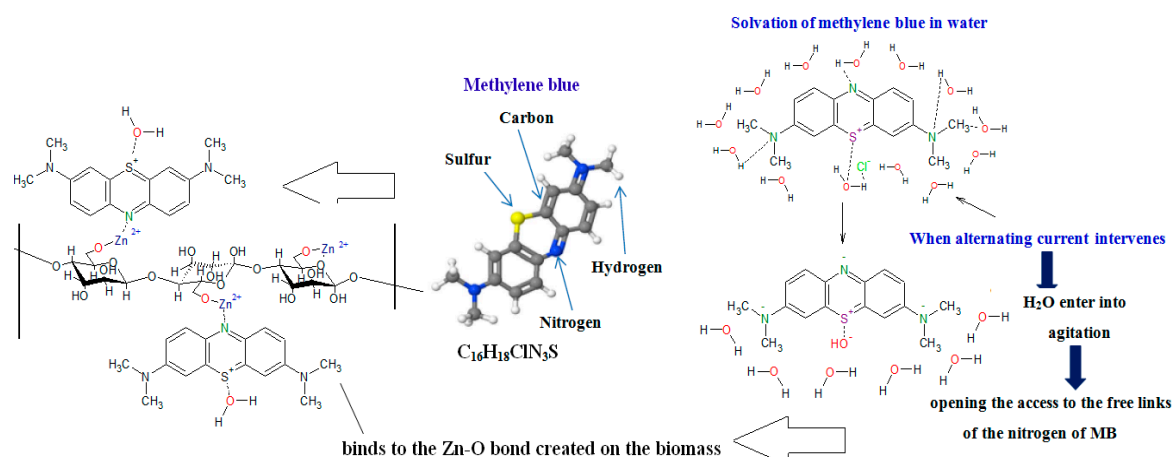


Figure 8. Possible pathway for the interactions between methylene blue and the synthesized hybrid material.

Figure 7 (Figure S2 in the complementary information) presents the possible pathway of the fixation of Zn^{2+} ions onto the *L.C* fibers in the presence and absence of AC.

For both methods used the Zn^{2+} ions generated from the dissolution of $\text{Zn}(\text{NO}_3)_2$ in water were fixed on the surface of the *L.C* through cellulose or hemicellulose, where oxygen is found, ensuring the creation of Zn-O bond on the biomass as confirmed by IR characterizations. The use of AC has enhanced the access of the Zn^{2+} ions onto the fibers. Therefore, favoring the participation of all Zn^{2+} ions presents in solution in the creation of Zn-O and Zn-O-C bonds. These findings can be confirmed by IR characterizations. The band located at 1383 cm^{-1} appears from 1% of Zn^{2+} for the hybrid material synthesized under AC, while it appears only for 4 % of Zn^{2+} for the hybrid materials synthesized in absence of AC ensuring an increase in the number of sites available onto the hybrid material surface.

Figure 8 (Figure S3 in the complementary information) presents the proposal of a possible pathway of the interactions between MB and the synthesized hybrid material and the effect of alternating current on the proposal process.

Water solvates MB by making hydrogen bridges hydrogen obtained from and nitrogen obtained from MB and a polar bond between oxygen and sulfur (π - π Bond).

When alternating current intervenes, the molecules of H₂O enter into agitation opening the access to the free links of the nitrogen of MB which subsequently binds to the Zn-O bond created on the biomass.

4. Conclusions

We have successfully synthesized a performing hybrid material based on *Luffa cylindrica* fibers and different percentage of zinc oxide (1%, 2%, and 4%) by an easy precipitation method under AC. The fast and efficient pollutant removals are the basic benefits of this research. Results confirmed clearly the effect of AC on the modification of acidic-basic properties of the L.C compared to the pure one. The addition of the different percentage of Zn²⁺ (1%, 2%, and 4%) has increased the basicity of the surface functionality by increasing the pH_{pzc}. Boehm titration indicated that the use of AC in the preparation of the hybrid materials has decreased the carboxylic and phenolic groups and increased the lactonic group. The presence of more lactonic groups has increased the density of the negative charge on the hybrid material surface which will play a crucial effect on the positively charged dye (MB) biosorption capacity. AC has increased the fixation and the distribution of Zn²⁺ into the L.C fibers by increasing the sites' number as confirmed by B.S (1, α). Physicochemical analyses revealed a prominent decrease in the COD, the TOC and the turbidity of the treated industrial textile wastewater, complied with the Tunisian Standards TN-106-02. The treated textile wastewater can be discharged to any receiving water. Furthermore, the germination indexes are higher than 50% confirmed their suitability to agricultural use.

Supplementary Materials: The following are available online at <http://www.mdpi.com/2073-4441/11/7/1326/s1>, Figure S1: Evolution of the % GI after coupling biosorption with AC using pure L.C and hybrid material L.C + 4% Zn²⁺ synthesized in presence and absence of AC, Figure S2: Possible pathway for the fixation of Zn²⁺ onto the L.C surface, Figure S3: Possible pathway for the interactions between methylene blue and the synthesized hybrid material, Table S1: Comparative results for the B.S model.

Author Contributions: Conceptualization, A.O., A.K. and M.S.; Formal analysis, A.O., A.K. and M.S.; Methodology, A.O.; resources, A.O., A.K., M.S. and R.B.; Writing—Original Draft preparation, A.O.; Writing—Review and Editing, A.O., A.K., M.S., R.B. and M.V.

Funding: This study was supported by 5TOI_EWAS project funded by the European Union's Horizon 2020 Research and Innovation Program under Grant Agreement No. 692523.

Acknowledgments: The authors express their sincere thanks to the Laboratory of Energy and Materials (High School of Sciences and technology of Hammam Sousse) for the financial support and the Unitat de Química Analítica, Departament de Química, Centre Grup de Tècniques de Separació en Química (GTS), Universitat Autònoma de Barcelona, Bellaterra, Spain.

Conflicts of Interest: The authors declare no conflict of interest.

References

1. Adegoke, K.A.; Bello, O.S. Dye sequestration using agricultural wastes as adsorbents. *Water Resour. Ind.* **2009**, *12*, 8–24. [[CrossRef](#)]
2. Laasri, L.; Elamrani, M.K.; Cherkaoui, O. Removal of two cationic dyes from a textile effluent by filtration-adsorption on woodsawdust. *Environ. Sci. Pollut. Res.-Int.* **2007**, *14*, 237–240. [[CrossRef](#)] [[PubMed](#)]
3. Abidin, F.C.Z.A.; Rahmat, N.R. Multi-stage ozonation and biological treatment for removal of azo dye industrial effluent. *Int. J. Environ. Sci. Dev.* **2010**, *1*, 193–198.
4. Othmani, A.; Kesraoui, A.; Seffen, M. The alternating and direct current effect on the elimination of cationic and anionic dye from aqueous solutions by electrocoagulation and coagulation flocculation. *Euro-Mediterr. J. Environ. Integr.* **2017**, *2*, 2–6. [[CrossRef](#)]
5. Selmi, T.; Sanchez-Sanchez, A.; Gadonneix, P.; Jagiello, J.; Seffen, M.; Sammouda, H.; Celzard, A.; Fierro, V. Tetracycline removal with activated carbons produced by hydrothermal carbonisation of Agave americana fibres and mimosa tannin. *Ind. Crop. Prod.* **2018**, *115*, 146–157. [[CrossRef](#)]

6. Căilean, D.; Barjoveanu, G.; Musteret, C.P.; Sulitanu, N.; Manea, L.R.; Teodosiu, C. Reactive dyes removal from wastewater by combined advanced treatment. *Environ. Eng. Manag. J.* **2009**, *8*, 503–511. [[CrossRef](#)]
7. Vasudevan, S.; Lakshmi, J.; Sozhan, G. Effects of alternating and direct current in electrocoagulation process on the removal of cadmium from water. *J. Hazard. Mater.* **2011**, *192*, 26–34. [[CrossRef](#)] [[PubMed](#)]
8. Vijayageetha, V.A.; Rajan, A.P.; Arockiaraj, S.P.; Annamalai, V.; Janakarajan, V.N.; Balaji, M.D.S.; Dheenadhayalan, M.S. Treatment study of dyeing industry effluents using reverse osmosis technology. *Res. J. Recent Sci.* **2014**, *3*, 58–61.
9. Elaissaoui, I.; Akrou, H.; Grassini, S.; Fulginiti, D.; Bousselmi, L. Role of SiO_x interlayer in the electrochemical degradation of Amaranth dye using SS/PbO₂ anodes. *Mater. Des.* **2016**, *10*, 633–643. [[CrossRef](#)]
10. Vendruscolo, F.; Ferreira, G.L.R.; Filho, N.R.A. Biosorption of hexavalent chromium by microorganisms. *Int. Biodeterior. Biodegrad* **2017**, *119*, 87–95. [[CrossRef](#)]
11. Davis, T.A.; Volesky, B.; Mucci, A. A review of the biochemistry of heavy metal biosorption by brown algae. *Water Res.* **2003**, *37*, 4311–4330. [[CrossRef](#)]
12. Atar, N.; Olgun, A.; Colk, F. Thermodynamic, Equilibrium and Kinetic Study of the Biosorption of Basic Blue 41 using *Bacillus maceran*. *Eng. Life Sci.* **2008**, *8*, 499–506. [[CrossRef](#)]
13. Champenois, W.; Borges, A.V. Determination of dimethyl sulfonio propionate and dimethyls ulfoxide in Posidonia oceanic leaf tissue. *MethodsX* **2019**, *6*, 56–62.
14. Mbarki, F.; Kesraoui, A.; Seffen, M.; Ayrault, P. Kinetic, thermodynamic and adsorption behavior of cationic and anionic dyes onto Corn stigmata: Non-linear and stochastic analyses. *Water Air Soil* **2018**, *229*, 95. [[CrossRef](#)]
15. Kesraoui, A.; Mabrouk, A.; Seffen, M. Valuation of Biomaterial: *Phragmites australis* in the Retention of Metal Complexed Dyes. *Am. J. Environ. Sci.* **2017**, *3*, 266–276. [[CrossRef](#)]
16. Demir, H.; Top, A.; Balkose, D.; Ulk, S. Dye adsorption behavior of Luffa cylindrica fibers. *J. Hazard. Mater.* **2008**, *153*, 389–394. [[CrossRef](#)] [[PubMed](#)]
17. Wang, S.; Boyjoo, Y.; Choueib, Z.H.A. Removal of dyes from aqueous solution using fly ash and red mud. *Water Res.* **2015**, *39*, 129–138. [[CrossRef](#)]
18. Hachani, R.; Sabir, N.S.; Zohra, K.F.; Nesrine, M.N. Performance Study of a Low-cost Adsorbent-Raw Date Pits-for Removal of Azo Dye in Aqueous Solution. *Water Environ. Res.* **2017**, *98*, 827–839. [[CrossRef](#)]
19. El Shahawy, A.; Ghada Heikal, G. Organic pollutants removal from oily wastewater using clean technology economically, friendly biosorbent (*Phragmites australis*). *Ecol. Eng.* **2018**, *122*, 207–218. [[CrossRef](#)]
20. Osman, C. Synthèse De Nouveaux Matériaux Hybrides Pour Les Catalyses En Atrp Supporté Du Méthacrylate De Méthyle. Ph.D. Thesis, University of Pierre and Marie Curie, Paris, France, 2014.
21. Shivaramakrishnan, B.; Gurumurthy, B.; Balasubramanian, A. Potential biomedical applications of metallic nanobiomaterials: A review. *Int. J. Pharm. Sci. Res.* **2017**, *8*, 98500.
22. Ye, J.D.; Gu, S.L.; Qin, F.; Zhu, S.M.; Liu, S.M.; Zhou, X.; Liu, W.; Hu, L.Q.; Zhang, R.; Shi, Y.; et al. MOCVD growth and properties of ZnO films using dimethylzinc and oxygen. *Appl. Phys. A* **2005**, *81*, 809–812. [[CrossRef](#)]
23. Tului, M.A.; Bellucci, A.; Migliozi, G. Zinc oxide targets for magnetron sputtering PVD prepared by plasma spray. *Surf. Coat. Technol.* **2005**, *205*, 1070–1073. [[CrossRef](#)]
24. Zamiri, R.; Zakaria, H.A.; Ahangar, M.; Zak, A.K.; Drummen, G.P.C. Aqueous starch as a stabilizer in zinc oxide nanoparticle synthesis via laser ablation. *J. Alloys Compd.* **2012**, *516*, 41–48. [[CrossRef](#)]
25. Perelshtein, L.; Applerot, G.; Perkash, N.; Wehrschetz-Sigl, E.; Hasmann, A.; Guebitz, G.M.; Gedanken, A. Antibacterial Properties of an In Situ Generated and Simultaneously Deposited Nanocrystalline ZnO on Fabrics. *ACS Appl. Mater. Interfaces* **2008**, *1*, 361–366. [[CrossRef](#)] [[PubMed](#)]
26. Hu, W.; Chen, S.; Zhou, B.; Wang, H. Facile synthesis of ZnO nanoparticles based on bacterial cellulose. *Mater. Sci. Eng. B* **2010**, *170*, 88–92. [[CrossRef](#)]
27. Ching, C.G.; Lee, S.C.; Ooi, P.K.; Ng, S.S.; Hassan, Z.; Hassan, H.A.; Abdullah, M.J. Optical and structural properties of porous zinc oxide fabricated via electrochemical etching method. *Mater. Sci. Eng. B* **2013**, *178*, 956–959. [[CrossRef](#)]
28. Chen, C.Y.; Chang, H.W.; Shih, S.J.; Tsay, C.Y.; Chang, C.J.; Lin, C.K. High super capacitive stability of spray pyrolyzed ZnO-added manganese oxide coatings. *Ceram. Int.* **2013**, *39*, 1885–1892. [[CrossRef](#)]
29. Brinker, C.J.; Scherer, G.W. *Sol-Gel Science: The Physics and Chemistry of Sol-Gel Processing Academic*; ET Press: Frankfurt, Germany, 1990.

30. Kesraoui, A.; Bouzaabia, S.; Seffen, M. The combination of Luffa cylindrical fibers and metal oxides offers a highly performing hybrid fiber material in water decontamination. *Environ. Sci. Pollut. Res.* **2018**, *26*, 11524–11534. [[CrossRef](#)]
31. Kesraoui, A.; Moussa, A.; Ali, G.B.; Seffen, M. Biosorption of alpacide blue from aqueous solution, by lignocellulosic biomass: *Luffa cylindrical* fibers. *Environ. Sci. Pollut. Res.* **2015**, *23*, 15832–15840. [[CrossRef](#)]
32. Shafei, A.; Nikzar, M.; Arami, M. Photocatalytic degradation of terephthalic acid using titania and zinc oxide ZnO photocatalysts comparative study. *Desalination* **2013**, *252*, 8–16. [[CrossRef](#)]
33. Kesraoui, A.; Selmi, T.; Seffen, M.; Brouer, F. Influence of alternating current on the adsorption of indigo carmine. *Environ. Sci. Pollut. Res.* **2016**, *24*, 9940–9950. [[CrossRef](#)] [[PubMed](#)]
34. Boumediene, M.; Benaïssa, H.; George, B.; Molina, S.; Merlin, A. Effects of pH and ionic strength on methylene blue removal from synthetic aqueous solutions by sorption onto orange peel and desorption study. *J. Mater. Environ. Sci.* **2018**, *9*, 1700–1711.
35. Goertzen, L.; ThériaultKim, S.D.; Oickle, M.A.; Tarasuk, C.A.; Andreas, A.H. Standardization of the Boehm titration. Part I. CO₂ expulsion and endpoint determination. *Carbon* **2010**, *48*, 1252–1261. [[CrossRef](#)]
36. Nava, J.L.; Quiroz, M.A.; Martinez-Huitle, C.A. Electrochemical treatment of synthetic wastewaters containing Alphazurine A dye: Role of electrode material in the color and COD removal. *J. Mex. Chem. Soc.* **2008**, *52*, 249–255.
37. Sharma, A.; Bhattacharya, S.; Sen, R.; Reddy, B.S.B.; Fecht, H.J.; Das, K.; Das, S. Influence of current density on microstructure of pulse electrodeposited tin coatings. *Mater. Charact.* **2012**, *68*, 22–32. [[CrossRef](#)]
38. Amrhar, O.; Nassali, H.; Elyoubi, M.S. Adsorption of a cationic dye, Methylene Blue, onto Moroccan Illitic Clay. *J. Mater. Environ. Sci.* **2015**, *6*, 3054–3065.
39. Brouers, F. Statistical foundation of empirical isotherms. *Open J. Stat.* **2014**, *4*, 687–701. [[CrossRef](#)]
40. Brouers, F. The fractal (BSf) kinetics equation and its approximations. *J. Mod. Phys.* **2014**, *5*, 1594–1601. [[CrossRef](#)]
41. Brouers, F.; Al-Musawi, T.J. On the optimal use of isotherm models for the characterization of biosorption of lead onto algae. *J. Mol. Liq.* **2015**, *212*, 46–51. [[CrossRef](#)]
42. Khot, L.R.; Sankaran, S.; Maja, J.M.; Ehsani, R.; Schuster, E.W. Applications of nanomaterials in agricultural production and crop protection: A review. *Crop Prot.* **2012**, *35*, 64–70. [[CrossRef](#)]
43. Antonio, R.; Tapia-Benavides, A.R.T.; Tlahuextl, M.; Tlahuext, H.; Galán-Vidal, C. Synthesis of Zn compounds derived from 1*H*-benzimidazol-2-ylmethanamine. *Arkivoc* **2008**, *5*, 172–186.
44. Xu, Q.; Chena, C.; Rosswurma, K.; Yaoa, T.; Janaswamy, S. A facile route to prepare cellulose-based films. *Carbohydr. Polym.* **2016**, *149*, 274–281. [[CrossRef](#)]
45. Vergnat, V. Matériaux Hybrides Organique-Inorganique Par Greffage Covalent De Polymères Sur Des Oxydes Métalliques. Ph.D. Thesis, University of Strasbourg, Strasbourg, France, 2011.
46. Zeleňák, V.; Vargová, Z.; Györyová, K. Correlation of infrared spectra of zinc (II) carboxylates with their structures. *Spectrochim. Acta A Mol. Biomol. Spectrosc.* **2007**, *66*, 262–272. [[CrossRef](#)]
47. Li, L.; Deng, J.; Deng, H.; Liu, Z.; Li, X. Preparation, characterization and antimicrobial activities of chitosan/Ag/ZnO blend films. *Chem. Eng. J.* **2010**, *160*, 378–382. [[CrossRef](#)]
48. Liu, X.F.; Sun, J.; Ren, J.; Curling, S.; Sun, R. Physicochemical characterization of cellulose from perennial leaves (*Lolium perenne*). *Carbohydr. Res.* **2006**, *341*, 2677–2687. [[CrossRef](#)] [[PubMed](#)]
49. Awala, H.; El-Roz, M.; Toufaily, J.; Mintova, S. Template-Free Nanosized EMT Zeolite Grown on Natural Luffa Fibers for Water Purification. *Adv. Porous Mater.* **2014**, *4*, 141–182. [[CrossRef](#)]
50. Arefi, M.R.; Zarchi, S.R. Synthesis of Zinc Oxide Nanoparticles and Their Effect on the Compressive Strength and Setting Time of Self-Compacted Concrete Paste as Cementitious Composites. *Int. J. Mol. Sci.* **2012**, *13*, 4340–4350. [[CrossRef](#)]
51. Wan, C.; Jian, L. Embedding ZnO nanorods into porous cellulose aerogels via a facile one-step low-temperature hydrothermal method. *Mater. Des.* **2015**, *83*, 620–625. [[CrossRef](#)]
52. Mahmoudi, K.H.; Hamdi, N.; Srasra, E. Kinetics and equilibrium studies on removal of methylene blue and methyl orange by adsorption onto activated carbon prepared from date pits—A comparative study. *Water Air Soil Pollut.* **2018**, *229*, 95. [[CrossRef](#)]
53. Cenens, J.; Schoonheydt, R.A. Visible spectroscopy of methylene blue on hectorite, laponite and barasym in aqueous suspension. *Clays Clay Min.* **1988**, *36*, 214–224. [[CrossRef](#)]

54. Kalmár, J.; Lente, G.; Fabian, I. Kinetics and mechanism of the adsorption of methylene blue from aqueous solution on the surface of a quartz cuvette by on-line UV-Vis spectrophotometry. *J. Dyes Pigments*. **2016**, *127*, 170–178. [[CrossRef](#)]
55. Selmi, T.; Seffen, M.; Sammouda, H.; Mathieu, S.; Jagiello, J.; Celzard, A.; Fierro, V. Physical meaning of the parameters used in fractal kinetic and generalised adsorption models of Brouers–Sotolongo. *Adsorption* **2017**, *24*, 11–27. [[CrossRef](#)]
56. Hammud, H.H.; Fayoumi, L.M.A.; Holail, H.; Mostafa, E.S.M.E. Biosorption studies of methylene blue by Mediterranean algae *Carolina* and its chemically modified forms. Linear and nonlinear models' prediction based on statistical error calculation. *Int. J. Chem.* **2011**, *3*, 147–163. [[CrossRef](#)]
57. Salleh, M.A.M.; Mahmoud, D.K.; Binti Awang Abu, N.A.; Abdul Karim, W.A.W.; Idris, A.B. Methylene blue adsorption from aqueous solution by langsung (*lansium domesticum*) peel. *J. Purity Util. React. Environ.* **2012**, *1*, 442–465.
58. Hamissa, A.M.B.; Brouers, F.; Ncibi, M.C.; Seffen, M. Kinetic Modeling Study on Methylene Blue Sorption onto *Agave americana* fibers: Fractal Kinetics and Regeneration Studies. *Sep. Sci. Technol.* **2013**, *48*, 2834–2842. [[CrossRef](#)]
59. Ncibi, M.C.; Mahjoub, B.; Seffen, M. Studies on the biosorption of textile dyes from aqueous solutions using *Posidonia Oceanica* (L.) leaf sheaths fibres. *Adsorpt. Sci. Technol.* **2006**, *24*, 461–473. [[CrossRef](#)]
60. García-Ávila, F.; Patiño-Chávez, J.; Zhinín-Chimbo, F.; Donoso-Moscoso, S.; del Pino, L.F.; Avilés-Añazco, L. Performance of *Phragmites Australis* and *Cyperus Papyrus* in the treatment of municipal wastewater by vertical flow subsurface constructed wetlands. *Int. Soil Water Conserv. Res.* **2019**. [[CrossRef](#)]
61. Dallel, D.; Kesraoui, A.; Seffen, M. Biosorption of cationic dye onto “*Phragmites australis*” fibers: Characterization and mechanism. *J. Environ. Chem. Eng.* **2018**, *6*, 6. [[CrossRef](#)]
62. Louhichi, G.; Bousselmi, L.; Ghrabi, A.; Khouni, I. Process optimization via response surface methodology in the physico-chemical treatment of vegetable oil refinery wastewater. *Environ. Sci. Pollut. Res.* **2018**, 1–19. [[CrossRef](#)]
63. Mendes, P.M.; Becker, R.; Corrêa, L.B.; Bianchi, I.; Dai Prá, M.A.; Lucia, T., Jr.; Corrêa, E.K. Phytotoxicity as an indicator of stability of broiler production residues. *J. Environ. Manag.* **2016**, *167*, 156–159. [[CrossRef](#)]



© 2019 by the authors. Licensee MDPI, Basel, Switzerland. This article is an open access article distributed under the terms and conditions of the Creative Commons Attribution (CC BY) license (<http://creativecommons.org/licenses/by/4.0/>).